Near-infrared–actuated devices for remotely controlled drug delivery

Brian P. Timko[a,b,c,1], Manuel Arruebo[d,e,1], Sahadev A. Shankarappa[f], J. Brian McAlvin[a], Obiajulu S. Okonkwo[a,c], Boaz Mizrahi[a,c], Cristina F. Stefanescu[a], Leyre Gomez[e], Jia Zhu[c], Angela Zhu[c], Jesus Santamaria[d,e], Robert Langer[b,c,2], and Daniel S. Kohane[a,2]

[a]Laboratory for Biomaterials and Drug Delivery, Department of Anesthesiology, Division of Critical Care Medicine, Boston Children's Hospital, Harvard Medical School, Boston, MA 02115; [b]Department of Chemistry and Chemical Engineering, Massachusetts Institute of Technology, Cambridge, MA 02142; [c]Koch Institute for Integrative Cancer Research, Massachusetts Institute of Technology, Cambridge MA 02139; [d]Networking Research Center in Bioengineering, Biomaterials and Nanomedicine, E-50018 Zaragoza, Spain; [e]Institute of Nanoscience of Aragón and Department of Chemical Engineering, University of Zaragoza, E-50018 Zaragoza, Spain; and [f]Center for Nanosciences and Molecular Medicine, Amrita Institute of Medical Sciences and Research Center, Kochi 682 041, India

Contributed by Robert Langer, December 6, 2013 (sent for review October 23, 2013)

A reservoir that could be remotely triggered to release a drug would enable the patient or physician to achieve on-demand, reproducible, repeated, and tunable dosing. Such a device would allow precise adjustment of dosage to desired effect, with a consequent minimization of toxicity, and could obviate repeated drug administrations or device implantations, enhancing patient compliance. It should exhibit low off-state leakage to minimize basal effects, and tunable on-state release profiles that could be adjusted from pulsatile to sustained in real time. Despite the clear clinical need for a device that meets these criteria, none has been reported to date to our knowledge. To address this deficiency, we developed an implantable reservoir capped by a nanocomposite membrane whose permeability was modulated by irradiation with a near-infrared laser. Irradiated devices could exhibit sustained on-state drug release for at least 3 h, and could reproducibly deliver short pulses over at least 10 cycles, with an on/off ratio of 30. Devices containing aspart, a fast-acting insulin analog, could achieve glycemic control after s.c. implantation in diabetic rats, with reproducible dosing controlled by the intensity and timing of irradiation over a 2-wk period. These devices can be loaded with a wide range of drug types, and therefore represent a platform technology that might be used to address a wide variety of clinical indications.

gold | nanoshell | poly(n-isopropylacrylamide) | ethylcellulose | diabetes

The majority of drug delivery systems that achieve prolonged release of drugs do so in a passive manner; drug release occurs in a more-or-less sustained manner irrespective of changing circumstances. In particular, the pattern of drug release is beyond the control of the patient or health professionals (1). However, there are many situations (e.g., endocrine disorders, pain) in which drug release would ideally be provided on demand, or in which the magnitude of drug release would best be readily titratable to a specific endpoint. Apart from allowing optimal matching of treatment to need, such control could reduce side effects by minimizing excessive dosing. Moreover, a device that is administered once (e.g., by surgery or injection) and then triggered remotely could increase patient compliance, particularly in cases in which conventional administration is painful or inconvenient, or for elderly or mentally disabled patients (1–4).

Recent advances in materials science have enabled systems that respond to external stimuli such as electromagnetic fields or ultrasound (1–4). They have been realized as microchips (5), liposomes (6), microparticles (7), nanoparticles (8), and macroscale polymers (9) that release loaded drugs when the stimulus is applied. In principle, these materials enable control over the dose and timing of drug release and therefore can be used to achieve complex drug release regimens not possible with conventional passive sustained-release systems. However, most triggered systems reported to date release drug only in a burst rather than in continuous fashion, or only function for a single release event, or exhibit a poor ratio between on- and off-state release kinetics, and/or lack reproducibility over multiple release cycles (2).

One way to address these shortcomings is with reservoir-based systems that contain many doses of drug. As they release only a small portion of their content after each activation, they can remain functional for weeks or months (10). Such devices are beginning to undergo clinical translation; in fact, an electrically activated microchip that released pulsatile doses was recently used to treat osteoporotic women in clinical trials (5). We have hypothesized that reservoirs capped by membranes with externally tunable permeability would be able to achieve any type of dosing profile—ranging from pulsatile to sustained—and could therefore be used clinically to treat a wide range of indications.

Recently, we reported a reservoir-based system capped by a nanocomposite membrane that became porous, and therefore permeable to drugs, upon activation by an oscillating magnetic field (11, 12). The on-state drug release rate of that device could be tuned by adjusting the geometry and composition of the membrane, and therefore could be engineered to match the corresponding clinical need. The device could achieve sustained release for at least 24 h, and triggered reproducibly over at least 10 cycles with minimal baseline leakage (11, 12).

In the present report, we demonstrate a device that is instead activated by a continuous-wave near-IR (NIR; 808 nm) trigger to

Significance

Devices that release a drug in response to a remote trigger would enable on-demand control of the timing and dose of drug released. They would allow the patient or physician to adjust therapy precisely to a target effect, thus improving treatment and reducing toxicity. We have developed implantable reservoirs that release a drug when irradiated with near-infrared laser light. The release rate was correlated to laser intensity, with negligible leakage between doses. Devices containing aspart, a fast-acting analog of insulin, were implanted in diabetic rats and were able to achieve glycemic control upon irradiation. Such devices can be loaded with a wide range of drugs to treat a variety of clinical indications.

Author contributions: B.P.T., M.A., S.A.S., J.S., and D.S.K. designed research; B.P.T., M.A., S.A.S., J.B.M., O.S.O., B.M., C.F.S., L.G., J.Z., and A.Z. performed research; B.P.T., M.A., S.A.S., J.B.M., O.S.O., J.S., R.L., and D.S.K. analyzed data; and B.P.T., M.A., J.S., R.L., and D.S.K. wrote the paper.

The authors declare no conflict of interest.

[1]B.P.T. and M.A. contributed equally to this work.

[2]To whom correspondence may be addressed. E-mail: rlanger@mit.edu or daniel.kohane@childrens.harvard.edu.

This article contains supporting information online at www.pnas.org/lookup/suppl/doi:10.1073/pnas.1322651111/-/DCSupplemental.

provide on-demand, repeated, reproducible, and titratable drug delivery over extended periods. Light offers distinct advantages over other triggers because it can be spatially selective (e.g., with a narrow beam) and because lasers or light-emitting diodes can be readily manufactured for point-of-care use, e.g., laser pointer-style devices. NIR is amenable to clinical translation because tissue is most transparent in that regime (13, 14), safe limits of NIR exposure have been established (15), and NIR light has been used clinically for in vivo imaging (16) and hyperthermic tumor treatment (17–19).

NIR-sensitive biomaterials frequently incorporate gold nanomaterials [e.g., shells (20), rods (21), or cages (22)] which readily absorb light within the NIR window and then convert a portion of that light to heat. Modulation of the irradiance allows continuous control of heat production and consequently of drug release from thermosensitive devices. For the devices studied in the present report, we used hollow gold nanoshells (AuNSs) because they are less likely to deform than gold nanorods (8) and have previously been used for other biomedical applications (23). Synthetic routes toward AuNSs have been well established, and their absorbance maxima can be tuned anywhere within the NIR window to match the wavelength of the excitation source (23, 24).

Results

Membrane Formulation. The key feature of the system is an impermeable membrane that becomes porous when irradiated with NIR light (Fig. 1*A*). The membrane consists of a hydrophobic ethylcellulose matrix containing gold nanoparticles that heat when NIR-irradiated, and a network of interconnected polymer nanoparticles that reversibly collapse when heated beyond a critical temperature, contracting to approximately one tenth their original diameter. Previously, we showed that membranes containing the same collapsible polymers could be triggered over at least 10 on/off cycles. Those membranes turned on with a 1- to 2-min time lag to changes in the ambient temperature, and turned off with a <10 min time lag (12).

Hollow AuNSs (Fig. 1*B*) capped with poly(vinyl pyrrolidone) (PVP) were synthesized by galvanically reducing Au(III) on sacrificial Co templates (25–27). AuNSs exhibited strong extinction at approximately 800 nm, and were stable in water and ethanol (Fig. 1*C*), making them compatible with our membrane fabrication process. AuNSs heated when irradiated with 808 nm continuous-wave laser light (*SI Appendix*, Fig. S1*A*), but exhibited negligible change in morphology or extinction spectra after at least 17 h of laser exposure (*SI Appendix*, Fig. S1 *B–D*). These AuNSs should exhibit the same biocompatibility (28) as other similarly sized gold nanomaterials, as residual Co was far below the accepted toxicology threshold (29) (*SI Appendix*, Figs. S2 and S3 and Table S1).

The thermosensitive components of the membrane, the copolymer nanogel (NG) particles, were synthesized from *N*-isopropylacrylamide, *N*-isopropylmethacrylamide, and acrylamide (11, 12) (Fig. 1*D*). We used a ratio of the three monomers that exhibits a collapse temperature slightly higher than 37 °C (12). When these particles were heated above that temperature, they reversibly shrank from approximately 800 nm diameter to <100 nm as the polymer became hydrophobic and the material dewetted (Fig. 1*E*).

Nanocomposite membranes 134 ± 14 μm thick (mean ± SD; $n = 72$; Fig. 1*F*) were cast by drying an ethanolic mixture containing PVP-stabilized AuNSs, NGs, and ethylcellulose in dishes. Cell types representative of the membranes' eventual in vivo milieu were exposed to the membranes and their constituent nanoparticles; cytotoxicity was minimal (30, 31) (*SI Appendix*, Fig. S4).

Irradiation with 808 nm laser light at 43 mW/cm^2 heated dry nanocomposite membranes loaded with 0.1 wt% AuNSs from

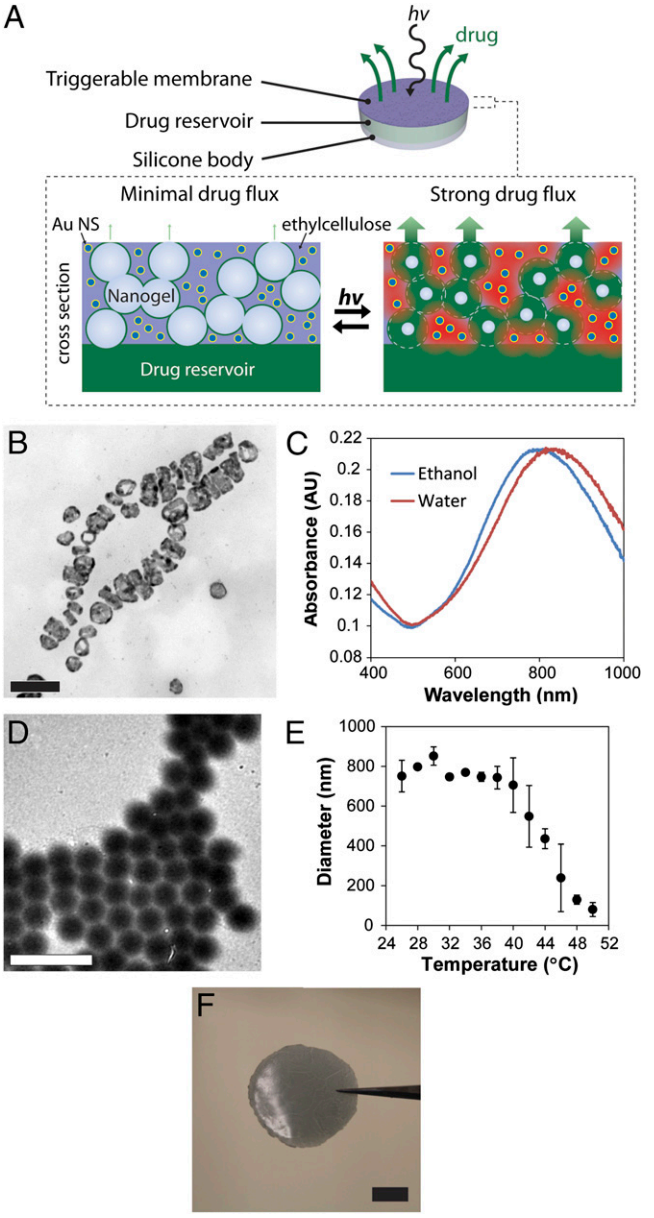

Fig. 1. Material properties. (*A*) Schematic of proposed device (*Upper*) and membrane cross-section (*Lower*). (*B*) Transmission EM image of hollow AuNSs. (Scale bar: 100 nm.) (*C*) UV-visible spectra of the same AuNSs suspended in water or ethanol. (*D*) Transmission electron micrograph of NG particles. (Scale bar: 2 μm.) (*E*) Effect of temperature on NG size, determined by differential light scattering ($n = 3$; data are means ± SD). (*F*) Photograph of a nanocomposite membrane. (Scale bar: 1 cm.)

room temperature to approximately 42.5 °C, whereas membranes without AuNSs heated negligibly (Fig. 2 *A* and *B*). Heating was linearly dependent on laser power flux over the range of 0 to 150 mW/cm^2 (Fig. 2*C*), implying that the extent of NG collapse, and therefore membrane permeability, might be continuously adjustable by laser power. Temperature under irradiation increased with AuNS loading (Fig. 2*D*, black trace), but plateaued at approximately 0.1 wt% AuNS. This was likely related to the fact 808 nm light transmittance through the membrane decreased from 31 ± 3% at 0.001 wt% AuNS loading to near-opacity at 0.2 wt% (Fig. 2*D*, red trace).

Membrane permeability was assessed by measuring the rate of fluorescein flux between two glass reservoirs containing sodium

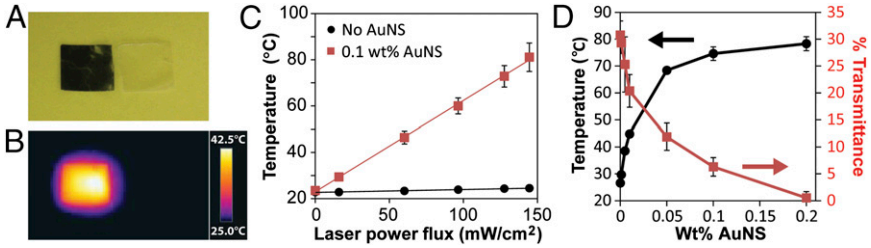

Fig. 2. Thermal characteristics. (*A*) Photograph of dry nanocomposite membranes containing 0.1 wt% AuNSs (*Left*) or no AuNSs (*Right*). (*B*) Thermal image of the same membranes uniformly irradiated with 808 nm light at 43 mW/cm^2. (*C*) Membrane temperature as a function of laser irradiance (n = 5). (*D*) Membrane temperature at 227 mW/cm^2 irradiance (black; left axis; n = 4) and transmittance at 808 nm (red; right axis; n = 8) as a function of AuNS content. Data are means ± SD.

fluorescein in PBS solution (donor side) or PBS solution alone (receptor side) (11, 12). Flux was triggered by direct heating via a water jacket, or by 808 nm laser irradiation. With direct heating over the range from 35 to 45 °C, the presence of AuNS did not affect flux across membranes containing NGs (Fig. 3*A*), indicating that the AuNSs did not interfere with NG collapse. Release rates began to plateau at approximately 43 °C, suggesting that the NGs were fully collapsed at that temperature. Membranes containing AuNSs without NGs exhibited negligible flux at all temperatures studied, demonstrating that AuNSs themselves do not introduce significant porosity into the membrane. For studies of laser-triggering (Fig. 3*B*), the membranes were maintained at 37 °C and irradiated between 0 and 580 mW/cm^2. Membranes containing 0.1 wt% or 0.025 wt% AuNS began to plateau in flux at approximately 350 mW/cm^2 (Fig. 3*B*), suggesting that the gel was almost fully collapsed. Comparison of the plateau regions in the temperature- and laser-triggered flux plots (Fig. 3 *A* and *B*) suggested that irradiances between 0 and 350 mW/cm^2 result in local membrane temperatures between approximately 37 and 43 °C (i.e., a temperature range over which the NGs collapse). Membranes containing less than 0.025 wt% AuNS were not fully collapsed at 350 mW/cm^2 (Fig. 3*C*), consistent with our observation that they heat less (Fig. 2*D*). Regardless of AuNS loading density, the relatively moderate temperatures required to achieve triggering are unlikely to damage biologic agents (e.g., proteins) as they diffuse through the membrane; for example, the specific activity of aspart was unaffected by loading into devices, irradiation, and release (*SI Appendix*, Fig. S5). Ideally, devices should contain at least 0.025 wt% AuNS because they require the lowest irradiance for triggering; the 350 mW/cm^2 required to turn them almost fully on (i.e., all NGs collapsed) is similar to or lower than power densities used in other biological applications (17, 18).

Device Design. Diabetic rats were to be treated with membrane-sealed devices loaded with a commercial formulation of aspart (NovoLog; Novo Nordisk), a fast-acting analog of insulin (32). Our design goal was to deliver 0.50 to 1.5 U per dose, which depresses the blood sugar level of diabetic rats (≥300 mg/dL) to normal levels (approximately 100 mg/dL) when administered by injection (33). Doses were to be delivered over 30-min on-state intervals, i.e., at release rates of 1.0 to 3.0 U/h. To achieve this target, we assessed devices with a range of membrane NG densities, aspart loading concentrations, and geometries, enabling us to realize devices with on-state release kinetics ranging over orders of magnitude (*SI Appendix*, Figs. S6 and S7 and Table S2). We used membranes with a high concentration of AuNSs, and therefore high sensitivity to light, and used irradiation at 570 mW/cm^2, as irradiation at 808 nm is attenuated by approximately 60% by rat skin ex vivo.

Devices with the desired release kinetics were 13 mm in diameter, contained approximately 200 μL aqueous drug solution, and were capped on one side with a nanocomposite membrane (29 wt% NG, 0.15 wt% AuNS) with a 70 mm^2 triggerable membrane surface area (Fig. 4 *A* and *B*). Each device was loaded

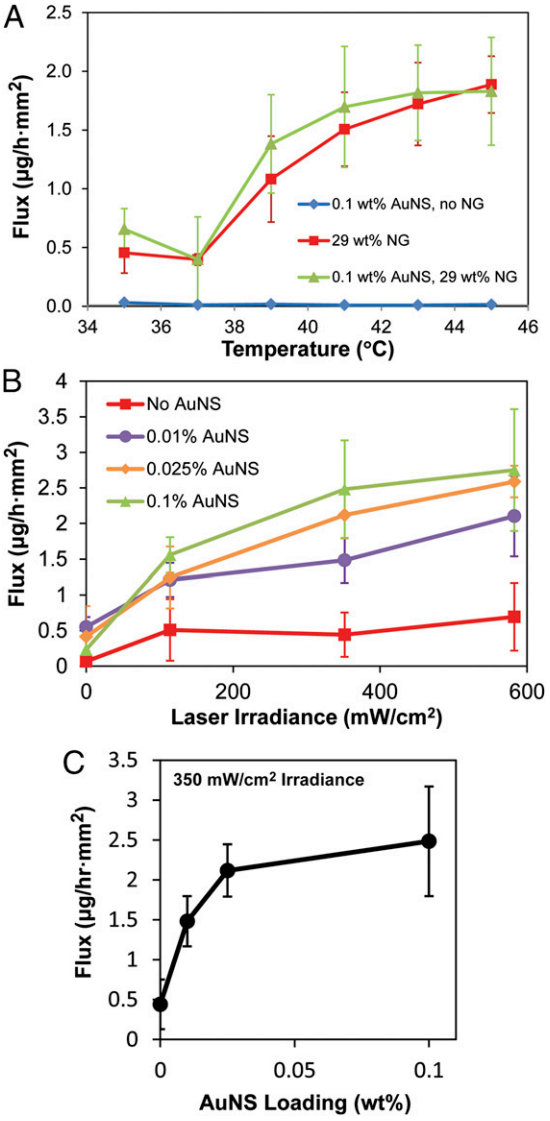

Fig. 3. Fluorescein transport studies. Flux across nanocomposite membranes as a function of (*A*) water bath temperature and (*B*) laser irradiance at constant 37 °C in a water bath. (*C*) Data in *B* were replotted to show the relationship between fluorescein flux and AuNS loading at 350 mW/cm^2 irradiance. For all data sets, n = 4. Data are means ± SD.

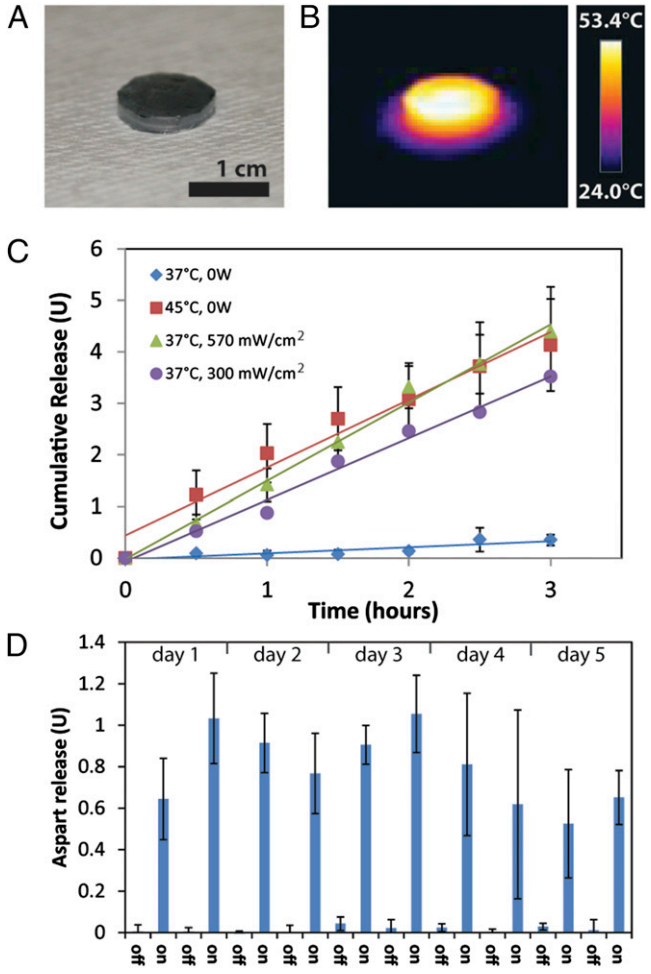

Fig. 4. Characteristics of aspart-loaded devices. (*A*) (*Left*) Photograph of a device capped with a nanocomposite membrane. (*B*) Thermal image of the same device uniformly irradiated with 808 nm light at 186 mW/cm^2. (*C*) The device was turned on by immersion in a 45 °C bath or laser irradiation at 570 mW/cm^2 or 300 mW/cm^2. In all cases, the release rate was constant over at least 3 h, and was much greater than release from the same devices in the off state (blue). For all traces, $n = 3$. Data are means ± SD. (*D*) Release from devices over 30-min dosing cycles. Devices were turned on with 570 mW/cm^2 laser light twice per day for 5 d. Off-state release was measured 30 min before laser triggering ($n = 3$); data are means ± SD.

with approximately 133 U (667 U/mL) of aspart. Devices immersed in PBS solution could be turned on by temperature (i.e., immersion in heated bath) or laser trigger; laser triggering at 570 mW/cm^2 yielded an average on-state release rate of 1.5 ± 0.3 U/h. Irrespective of triggering method, the devices exhibited sustained release kinetics in the on state over at least 3 h (Fig. 4*C*). Repeated dosing was demonstrated by 30-min dosing cycles triggered by laser irradiation (570 mW/cm^2) twice per day for 5 d (Fig. 4*D*). The average release during the on state was 0.8 ± 0.2 U. Measurements of release in the off state, taken during the 30 min before each triggered dose, showed reproducibly that devices released minimal aspart between dosing cycles (0.03 ± 0.01 U per 30-min interval); the on/off ratio was 30. A separate set of devices ($n = 11$) exhibited a similar on/off ratio when the off-state release rate (0.075 ± 0.06 U/h) was measured for approximately 1 h immediately following the on-state (2.1 ± 0.7 U/h), and so we inferred that the devices turned off quickly after triggering. These results demonstrated that devices could release drug in sustained or pulsatile fashion, and with low leakage in the off state; such functionality demonstrates the capability of our technology to achieve customizable, on-demand dosing.

In Vivo Studies. Devices were implanted s.c. in Sprague–Dawley rats rendered diabetic with streptozotocin (34) and triggered at least 1 d later with 30-min laser pulses. The blood glucose concentration decreased after each dose, with minimum concentration occurring 150 min after the start of the laser pulse. The magnitude of response was positively correlated to laser intensity, with reduction by 87 ± 17 mg/dL at 142 mW/cm^2 ($n = 3$) or 160 ± 40 mg/dL at 570 mW/cm^2 ($n = 6$). Aspart-filled devices that were not triggered by a laser pulse, or saline solution-filled control devices triggered at high irradiance (570 mW/cm^2), exhibited negligible effect on blood glucose level (Fig. 5 *A* and *B*). In a separate set of animals, implanted devices were triggered 1–3 and 14 d after implantation (570 mW/cm^2; 30 min; Fig. 5*C*), resulting in an average glucose reduction at 150 min of 140 ± 20 mg/dL ($n = 3$; $P = 0.7$; Fig. 5*D*). The reduction in serum glucose from the device was slower and of lesser magnitude than from s.c. injection of the same aspart dose (1 U; Fig. 5*E*), as would be expected from a triggered sustained release device vs. free drug (5).

Histology. We assessed tissue response to the implant and laser irradiation (*SI Appendix*, Figs. S8 and S9). Rats were implanted with devices (day 0) and divided into groups irradiated at 0 (control), 142, or 570 mW/cm^2. They were euthanized on day 4 after a single irradiation or on day 14 after four irradiations (days 1–3 and 14), and the device and surrounding tissues were collected for histological analysis. Cohorts irradiated with 0 or 142 mW/cm^2 [the latter is sufficient to trigger the device in vitro (Fig. 3*B*) and in vivo (Fig. 5*A*)] demonstrated healthy skin overlying the implanted device on days 4 and 14. On microscopy of stained sections, a mild inflammatory response was observed at both time points in the tissues directly adjacent to the device. Tissue reaction was consistent with what was reported for other implanted devices (11, 35).

At 570 mW/cm^2, ulceration was observed on the skin surface. On gross dissection, the device was surrounded by areas of hemorrhage (*SI Appendix*, Figs. S8 and S9). These injuries are seen in NIR laser burns (36, 37) and set an upper bound on acceptable dosing levels. Such high powers are not required to trigger our devices; however, safer therapies could be achieved by (*i*) using devices with higher on-state kinetics, which would require shorter irradiation times, (*ii*) designing devices with a lower on-state irradiation threshold, or (*iii*) using a pulsed laser source, which also heats nanoparticles but causes less tissue damage (38).

Discussion and Conclusions

We have developed an implantable device that releases a drug when irradiated with NIR light, whereby the dose is controlled by the timing and intensity of the irradiation. Our device represents a significant advance in triggered drug release technology because of its unique combination of excellent reproducibility, low off-state leakage, range of drug release profiles, and noninvasive triggerability within the body. Of further importance is the fact that, by changing the composition and geometry of the membrane (e.g., thickness, NG loading, surface area), the dynamic range of release kinetics can be readily tuned to match the therapeutic window for the given indication.

Another distinct advantage of our system is that it is triggered with a relatively inexpensive and compact continuous-wave laser system that could be readily adapted for point-of-care systems. Future iterations might be achieved with a wearable or pen-style triggering device. Laser light is spatially selective, so different devices implanted at remote locations could be triggered independently. Because the devices are triggered by inductive

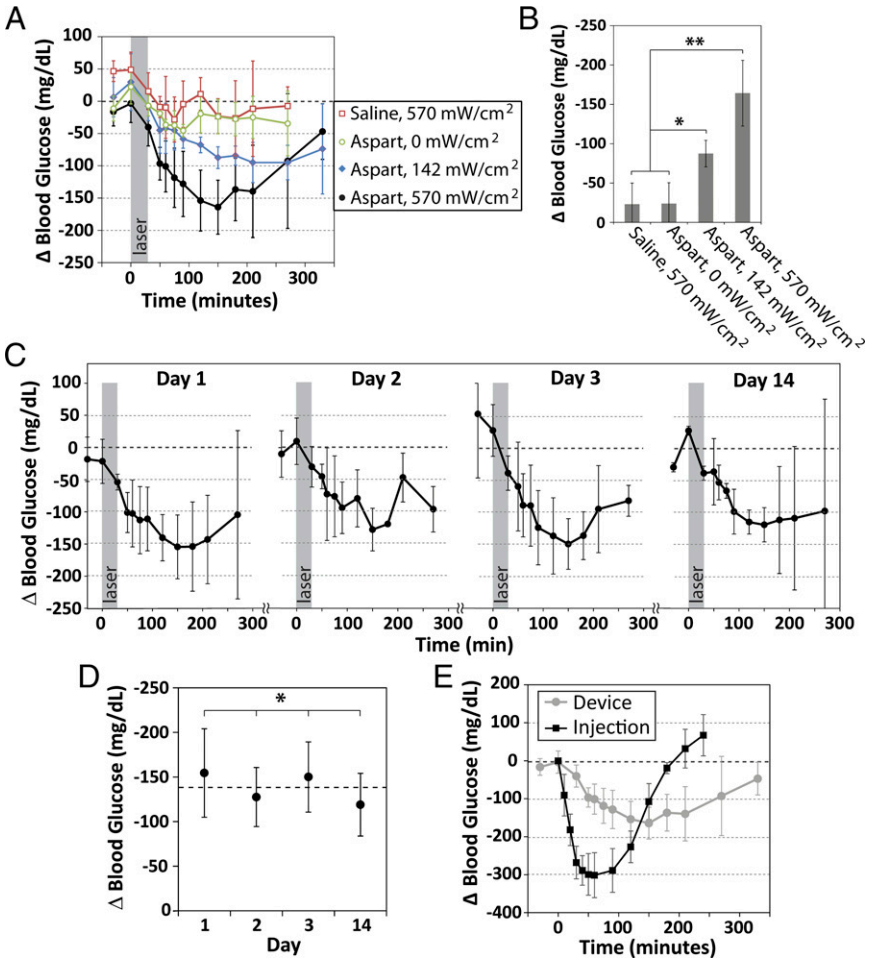

Fig. 5. Blood glucose control in vivo. (*A*) One day after device implantation, blood glucose levels were measured after triggered release from devices filled with saline ($n = 4$) or aspart solution by using an NIR trigger (30 min duration; gray box) of 0, 142, or 570 mW/cm^2 irradiance ($n = 4$, $n = 3$, and $n = 6$, respectively). (*B*) Summary of blood glucose data in *A* at 150 min (*$P < 0.03$ and **$P < 0.002$, two-tailed t test). (*C*) Serum glucose levels after repeated dosing at the same irradiance (gray box; 30 min duration; 570 mW/cm^2) on four separate occasions over 14 d ($n = 3$). (*D*) In the trials shown in *C*, the average depression at 150 min was 140 ± 20 mg/dL (dotted line) across all four doses (*$P = 0.7$, one-way ANOVA). (*E*) Comparison of serum glucose response after administering 1 U aspart by s.c. injection (black, $n = 4$) or by triggered release from devices (gray; $n = 6$; trace reproduced from *A*). The maximum glucose depression occurred at 60 min (injection) or 150 min (device). All data are means ± SD.

coupling with the light, they require no onboard power source or other logic.

Future improvements might enhance the safety and efficacy of our devices. The collapse temperature of the NG can be readily adjusted to temperatures higher than 37 °C to prevent accidental triggering, e.g., because of fever or hot weather (12). The device might also be fabricated with several isolated wells, or even tens or hundreds (5), to minimize leakage or burst release of the drug should a portion of the membrane break. Future devices should also have a much lower triggering threshold to avoid thermal injury after repeated dosing, especially for deep implants for which NIR attenuation will be more substantial than in the s.c. studies reported here. The size, geometry, and composition of the metallic nanostructures within the device should be assessed systematically to identify those that most efficiently convert light into heat; additionally, the distribution of nanomaterials throughout the membrane might be designed to maximize heat transfer between the gold and NG. Finally, fully bioresorbable devices might be achieved by replacing the ethylcellulose components with biodegradable materials (39, 40), although the degradation kinetics would need to be sufficiently slow to avoid uncontrolled release of remaining drug.

Here, for proof of concept, we released a drug for systemic delivery. However, this platform could readily be used for localized drug delivery (4). For example, it could be placed on a nerve, allowing the patient the capability for precise titration of local analgesia to match actual needs and circumstances. These devices can be used to deliver a wide range of drug types from small molecules to macromolecules (12), and therefore could be useful for treating a wide range of disorders.

Materials and Methods

A full description of Materials and Methods is provided in *SI Appendix*.

NG Synthesis. NG particles were synthesized using previously reported procedures (11, 41). In brief, *N*-isopropylacrylamide (0.6 g), *N*-isopropylmethacrylamide (0.8 g), acrylamide (50 mg) and *N*,*N*′-methylenebisacrylamide (80 mg) were dissolved in 150 mL deionized (DI) water. The solution and flask were degassed with a nitrogen or argon purge for 30 min and heated to 70 °C. Ammonium persulfate initiator (100 mg) was dissolved in 5 mL DI water and added to the solution at once with gentle stirring. The reaction proceeded for approximately 4 h, yielding an opaque white suspension of NG particles. The particles were dialyzed against DI water to remove unreacted monomer, then lyophilized. The resulting particles exhibited a hydrated diameter of approximately 800 nm and collapsed at temperatures greater than 37 °C.

Nanoshell Synthesis. Nanoshells were synthesized by reduction of Au(III) at the surface of sacrificial cobalt seeds (25). Cobalt chloride hexahydrate (38.1 mg) and sodium citrate tribasic dehydrate (47.1 mg) were mixed with 400 mL DI water in a round-bottom flask. The solution was purged with nitrogen or argon for 40 min. To the degassed solution was added 2.0 mL 1 wt% polyvinylpyrrolidone solution (55 kDa average molecular weight). Subsequent addition of 0.4 mL ice-cold 1 M sodium borohydride solution immediately reduced the cobalt, yielding a grayish solution. The suspension was purged for an additional 15 min to ensure complete oxidation of the borohydride. A total of 360 mL of the resulting Co nanoparticle solution was transferred to an open flask containing 120 mL of water and 180 μL 0.1M $HAuCl_4$. The mixture slowly turned blue-green over about 30 min. The resulting particles were concentrated, washed three times with 0.1 wt% PVP solution, then lyophilized and stored for further use.

Membrane Formulation. Lyophilized NGs and nanoshells were suspended in ethanol at concentrations of 50 mg/mL and 0.5 to 1 mg/mL, respectively. Ethylcellulose (Sigma-Aldrich) was dissolved in ethanol at a concentration of 10 wt%. The components were mixed together at the appropriate ratio, and the mixture was cast into six-well cell culture dishes (BD Falcon). The membranes were dried in a desiccator (Secador Auto Dessicator; Bel-Art Products) for approximately 3 d.

Laser Irradiation. For laser studies, we used an 808-nm diode laser (MDL-III-808, 0–2.5W continuous wave output; Optoengine) and a 400-μm fiberoptic cable. For some experiments, the fiberoptic was attached to a silica-lens collimator with a 22.2-mm aperture (CeramOptec Industries).

Sodium Fluorescein Flux Experiments. Studies were performed using glassware from PermeGear. For temperature studies, we used Side-bi-Side cells with water jacket adjusted to the appropriate temperature. For laser studies, we used custom-made Franz cells with water jacketed donor and receptor sides to avoid nonspecific heating by the laser. All laser studies were performed with the water jacket adjusted to 37 °C. For all studies, the donor side was filled with 10 mg/mL sodium fluorescein in PBS solution, and the receptor side was filled with PBS solution. For each data point, the flux was measured for approximately 2 h. The concentration of sodium fluorescein in the receptor chamber was measured by using a plate reader in fluorescence mode.

Devices. Device bodies were made with medical-grade silicone tubing (HelixMark, 0.375-inch i.d./0.500-inch o.d.). The tubes were capped on one side with a nanocomposite membrane (29 wt% NG, 0.15 wt% AuNS) and on the other side with an ethylcellulose film. Permabond 102, 105, or 200 was used for adhesion. NovoLog Insulin Aspart solution (Novo Nordisk) was concentrated to 667 U/mL and injected into sealed devices (approximately 200 μL, 133 U per device). Control devices were filled with saline solution (0.9% NaCl, wt/vol). Devices were soaked in PBS solution at 37 °C overnight, then cycled through approximately five on/off priming cycles before release studies. In vitro release was quantified with a Bradford protein assay (Bio-Rad).

Statistics. All *P* values were calculated by an unpaired, two-tailed *t* test or one-way ANOVA by using GraphPad InStat software (GraphPad). All data are means ± SD.

ACKNOWLEDGMENTS. The authors thank D. Bell for help with microscopy and D. Zurakowski, B. Tang, and G. Traverso for useful discussions. This research was funded by National Institutes of Health (NIH) Grant GM073626 (to D.S.K.), a Sanofi Biomedical Innovation Funding Award through the MIT Center for Biomedical Innovation (to D.S.K. and R.L.), and a Ruth L. Kirschstein National Research Service Award fellowship, NIH Award F32GM096546 (to B.P.T.). This work was performed in part at the Center for Nanoscale Systems (CNS), a member of the National Nanotechnology Infrastructure Network, which is supported by the National Science Foundation under Award ECS-0335765. CNS is part of Harvard University.

1. Timko BP, et al. (2011) Advances in drug delivery. *Annu Rev Mater Res* 41(41):1–20.
2. Timko BP, Dvir T, Kohane DS (2010) Remotely triggerable drug delivery systems. *Adv Mater* 22(44):4925–4943.
3. Timko BP, Kohane DS (2012) Materials to clinical devices: Technologies for remotely triggered drug delivery. *Clin Ther* 34(11):S25–S35.
4. Timko BP, Kohane DS (2013) Drug-delivery systems for tunable and localized drug release. *Isr J Chem* 53:728–736.
5. Farra R, et al. (2012) First-in-human testing of a wirelessly controlled drug delivery microchip. *Sci Transl Med* 4(122):22ra21.
6. Wu G, et al. (2008) Remotely triggered liposome release by near-infrared light absorption via hollow gold nanoshells. *J Am Chem Soc* 130(26):8175–8177.
7. Epstein-Barash H, et al. (2010) A microcomposite hydrogel for repeated on-demand ultrasound-triggered drug delivery. *Biomaterials* 31(19):5208–5217.
8. Wijaya A, Schaffer SB, Pallares IG, Hamad-Schifferli K (2009) Selective release of multiple DNA oligonucleotides from gold nanorods. *ACS Nano* 3(1):80–86.
9. Sershen SR, Westcott SL, Halas NJ, West JL (2000) Temperature-sensitive polymer-nanoshell composites for photothermally modulated drug delivery. *J Biomed Mater Res* 51(3):293–298.
10. Stevenson CL, Santini JT, Jr., Langer R (2012) Reservoir-based drug delivery systems utilizing microtechnology. *Adv Drug Deliv Rev* 64(14):1590–1602.
11. Hoare T, et al. (2009) A magnetically triggered composite membrane for on-demand drug delivery. *Nano Lett* 9(10):3651–3657.
12. Hoare T, et al. (2011) Magnetically triggered nanocomposite membranes: A versatile platform for triggered drug release. *Nano Lett* 11(3):1395–1400.
13. Weissleder R (2001) A clearer vision for in vivo imaging. *Nat Biotechnol* 19(4):316–317.
14. Simpson CR, Kohl M, Essenpreis M, Cope M (1998) Near-infrared optical properties of ex vivo human skin and subcutaneous tissues measured using the Monte Carlo inversion technique. *Phys Med Biol* 43(9):2465–2478.
15. American National Standards Institute and Laser Institute of America (2000) *American National Standard for Safe Use of Lasers* (Laser Institute of America, Orlando, FL).
16. Sevick-Muraca EM (2012) Translation of near-infrared fluorescence imaging technologies: Emerging clinical applications. *Annu Rev Med* 63(63):217–231.
17. Gobin AM, et al. (2007) Near-infrared resonant nanoshells for combined optical imaging and photothermal cancer therapy. *Nano Lett* 7(7):1929–1934.
18. Huang X, El-Sayed IH, Qian W, El-Sayed MA (2006) Cancer cell imaging and photothermal therapy in the near-infrared region by using gold nanorods. *J Am Chem Soc* 128(6):2115–2120.
19. Morton JG, Day ES, Halas NJ, West JL (2010) Nanoshells for photothermal cancer therapy. *Methods Mol Biol* 624:101–117.
20. Hirsch LR, et al. (2006) Metal nanoshells. *Ann Biomed Eng* 34(1):15–22.
21. Huang XH, Neretina S, El-Sayed MA (2009) Gold nanorods: From synthesis and properties to biological and biomedical applications. *Adv Mater* 21(48):4880–4910.
22. Xia Y, et al. (2011) Gold nanocages: From synthesis to theranostic applications. *Acc Chem Res* 44(10):914–924.
23. Zhang JZ (2010) Biomedical applications of shape-controlled plasmonic nanostructures: A case study of hollow gold nanospheres for photothermal ablation therapy of cancer. *J Phys Chem Lett* 1(4):686–695.
24. Dreaden EC, Alkilany AM, Huang XH, Murphy CJ, El-Sayed MA (2012) The golden age: Gold nanoparticles for biomedicine. *Chem Soc Rev* 41(7):2740–2779.
25. Schwartzberg AM, Olson TY, Talley CE, Zhang JZ (2006) Synthesis, characterization, and tunable optical properties of hollow gold nanospheres. *J Phys Chem B* 110(40):19935–19944.
26. Prevo BG, Esakoff SA, Mikhailovsky A, Zasadzinski JA (2008) Scalable routes to gold nanoshells with tunable sizes and response to near-infrared pulsed-laser irradiation. *Small* 4(8):1183–1195.
27. Preciado-Flores S, et al. (2011) Highly reproducible synthesis of hollow gold nanospheres with near infrared surface plasmon absorption using PVP as stabilizing agent. *J Mater Chem* 21(7):2344–2350.
28. Cebrián V, et al. (2013) Enhancing of plasmonic photothermal therapy through heat-inducible transgene activity. *Nanomedicine* 9(5):646–656.
29. Syracuse Research Corporation and US Agency for Toxic Substances and Disease Registry (2004) *Toxicological Profile for Cobalt* (US Department of Health and Human Services, Atlanta).
30. Kohane DS, Langer R (2010) Biocompatibility and drug delivery systems. *Chemical Science* 1(4):441–446.
31. Naahidi S, et al. (2013) Biocompatibility of engineered nanoparticles for drug delivery. *J Control Release* 166(2):182–194.
32. Brange J, Volund A (1999) Insulin analogs with improved pharmacokinetic profiles. *Adv Drug Deliv Rev* 35(2-3):307–335.
33. Plum A, Agerso H, Andersen L (2000) Pharmacokinetics of the rapid-acting insulin analog, insulin aspart, in rats, dogs, and pigs, and pharmacodynamics of insulin aspart in pigs. *Drug Metab Dispos* 28(2):155–160.
34. Lenzen S (2008) The mechanisms of alloxan- and streptozotocin-induced diabetes. *Diabetologia* 51(2):216–226.
35. LaVan DA, et al. (2005) In vivo evaluation of tetrahedral amorphous carbon. *Biomaterials* 26(5):465–473.
36. Museux N, Perez L, Autrique L, Agay D (2012) Skin burns after laser exposure: Histological analysis and predictive simulation. *Burns* 38(5):658–667.
37. Chen B, Thomsen SL, Thomas RJ, Oliver J, Welch AJ (2008) Histological and modeling study of skin thermal injury to 2.0 microm laser irradiation. *Lasers Surg Med* 40(5):358–370.
38. Sawa M, et al. (2004) Application of femtosecond ultrashort pulse laser to photodynamic therapy mediated by indocyanine green. *Br J Ophthalmol* 88(6):826–831.
39. Domb AJ, Kost J, Wiseman DM (1997) *Handbook of Biodegradable Polymers* (Harwood, Amsterdam).
40. Tamada JA, Langer R (1993) Erosion kinetics of hydrolytically degradable polymers. *Proc Natl Acad Sci USA* 90(2):552–556.
41. Das M, Zhang H, Kumacheva E (2006) Microgels: Old materials with new applications. *Annu Rev Mater Res* 36:117–142.